Feature-Tracking MRI Fractal Analysis of Right Ventricular Remodeling in Adults with Congenitally Corrected Transposition of the Great Arteries

Feature-Tracking MRI Fractal Analysis of Right Ventricular Remodeling in Adults with Congenitally Corrected Transposition of the Great Arteries

Masateru Kawakubo, PhD • Michinobu Nagao, MD • Umiko Ishizaki, MD • Yumi Shiina, MD •
Kei Inai, MD • Yuzo Yamasaki, MD • Masami Yoneyama, MT • Shuji Sakai, MD

From the Department of Health Sciences, Faculty of Medical Sciences (M.K.), and Department of Clinical Radiology, Graduate School of Medical Sciences (Y.Y.), Kyushu University, Fukuoka, Japan; Department of Diagnostic Imaging and Nuclear Medicine (M.N., U.I., S.S.) and Department of Pediatric Cardiology and Adult Congenital Cardiology (Y.S., K.I.), Tokyo Women's Medical University, 8-1 Kawada-cho, Shinjuku-ku, Tokyo, Japan; and Philips Japan, Tokyo, Japan (M.Y.). Received February 4, 2019; revision requested March 13; revision received July 22; accepted August 1. **Address correspondence to** M.N. (e-mail: *nagao.michinobu@twmu.ac.jp*).

Purpose: To assess a recently available technique for quantification of right ventricular (RV) trabeculae that is based on fractal analysis performed by using cardiac MRI feature tracking, in patients with congenitally corrected transposition of the great arteries (cc-TGA).

Materials and Methods: A total of 19 patients (eight men, 11 women; mean age, 35 years ± 10 [standard deviation]) with consecutive cc-TGA who underwent cardiac MRI were enrolled in the study. For analysis, patients were divided into two groups: six patients (four men, two women; mean age, 34 years ± 14) with an end-systolic RV volume index higher than 72 mL/m² (indicative of adverse RV remodeling) and 13 patients (four men, nine women; mean age, 36 years ± 9) in whom this index was lower than or equal to 72 mL/m² (indicative of adapted RV). The following outcomes were quantified in the midsection of the RV: fractional fractal dimension (FD) and diastolic FD, circumferential strain, and radial strain. Receiver operating characteristic (ROC) analysis was performed to determine the cutoff FD values for the detection of adverse RV remodeling. Correlations among fractional FD, diastolic FD, circumferential strain, and radial strain were calculated by using Pearson correlation coefficient (r) analysis.

Results: The following ROC values were identified for fractional and diastolic FD: cutoff, 0.09 and 1.39, respectively; area under the ROC curve, 0.95 and 0.68, respectively; sensitivity, 1.00 and 0.33, respectively; and specificity, 0.92 and 1.00, respectively. Fractional FD correlated with circumferential strain and radial strain (r = –0.70 and 0.69, respectively; P < .01), as did diastolic FD (r = 0.37 and –0.38, respectively; P < .05).

Conclusion: The fractional FD derived from cardiac MRI feature-tracking analysis correlates with adverse RV remodeling, including a changed strain pattern and trabeculae, in patients with cc-TGA.

©RSNA, 2019

In congenitally corrected transposition of the great arteries (cc-TGA), the anatomic right ventricle (RV) connects the left atrium to the aorta and provides systemic circulation. However, because the RV wall is thinner than the left ventricle (LV) wall, the RV may be poorly equipped to deal with aortic pressures after correction. As a result, the systemic RV becomes thick and dilated under long-term pressure (1–3); this condition is known as RV remodeling (4). Consequently, RV failure often occurs in patients with cc-TGA during adulthood. The formation of trabeculae is considered to be the epiphenomenon of RV remodeling, resulting in an anatomic RV phenotype similar to noncompaction ventricular myocardium. Captur et al (5–7) reported on the usefulness of fractal analysis, as performed with cardiac MRI during the end-diastolic phase, in quantifying LV trabeculae, noting a greater fractal dimension (FD) in patients with LV noncompaction than in those with hypertrophic cardiomyopathy. In addition, in adult patients with cc-TGA, the development of trabeculae in the systemic RV might be a specific marker of RV remodeling. However, in healthy adults, a more developed formation of trabeculae is commonly observed in the RV, as

compared with the formation in the LV. Therefore, given that fractal analysis occurs in the end-diastolic phase, in the quantification of trabeculae formation in the subaortic RV in patients with cc-TGA, the structural changes associated with remodeling may not be fully captured.

Strain analysis performed by using cardiac MRI feature tracking is a semiautomatic method that has been shown to be useful for characterizing structural changes of the heart in adults with congenital heart disease, including cc-TGA (8–11). This method of analysis has been used to demonstrate changes in the strain pattern of the subaortic RV, with circumferential strain (CS) becoming dominant over longitudinal strain, as is normal for the systemic LV (12). This change in the strain pattern could serve as an additional marker of RV remodeling under long-term systemic load.

Fractal analysis to assess the formation of LV trabeculae has been performed to discriminate isolated LV noncompaction and dilated cardiomyopathy (13). However, the clinical importance of RV trabeculae in adults with cc-TGA is not well understood. We hypothesized that the formation of trabeculae in the RV in adults with cc-TGA

Abbreviations

cc-TGA = congenitally corrected transposition of the great arteries, CI = confidence interval, CS = circumferential strain, FD = fractal dimension, ICC = intraclass correlation coefficient, LV = left ventricle, ROC = receiver operating characteristic, RS = radial strain, RV = right ventricle

Summary

The results of fractal analysis performed by using feature-tracking cardiac MRI correlated with adverse remodeling of the right ventricle, including changes in the strain pattern and trabeculae of the ventricle, in patients with congenitally corrected transposition of the great arteries.

Key Points

- In patients with congenitally corrected transposition of the great arteries, the fractional fractal dimension derived by using feature-tracking MRI, as compared with the conventional diastolic fractal dimension, facilitates a more accurate diagnosis of the development of right ventricular trabeculae owing to adverse remodeling.
- Fractal analysis performed by using feature-tracking MRI is a robust analytical method with high reproducibility.
- As fractal analysis performed with feature-tracking MRI does not require additional manual processing, it can be easily included with strain analysis in cardiac workflow analysis in clinical practice.

compensates for pressure overload in the systemic ventricle and that this formation progresses parallel to RV overload or RV dysfunction. Thus, we proposed the use of a recently introduced method for quantification of RV trabeculae that is performed by using fractal analysis with cardiac MRI feature tracking and investigated the association with RV remodeling and myocardial strain in the RV.

Materials and Methods

Study Population

This two-center retrospective observational study was approved by the local ethics committee and conducted in accordance with the Declaration of Helsinki (1964). Written informed consent was obtained from all patients. All examinations, including cardiac MRI, were performed as part of the clinical workup for patients with declining cardiac function. No authors have financial conflicts of interest to disclose concerning this presentation. One author (M.Y.) is an employee of Philips Electronics Japan.

The data from 19 consecutive patients with cc-TGA (eight men, 11 women; mean age, 35 years ± 10 [standard deviation]) who had systemic RV and were examined between March 2013 and March 2018 were included in the analysis. All patients were older than 18 years and determined to be clinically stable. In this group, 10 patients had undergone a conventional Rastelli procedure. After this surgery, the anatomic LV was connected to the pulmonary artery by an extracardiac conduit. On the basis of the definition of *RV remodeling* in pulmonary hypertension in a recent echocardiography study (14), patients were divided into two groups: six patients (four men, two women; mean age, 34 years ± 14 [standard deviation]) with an RV end-systolic volume

index higher than 72 mL/m^2 (indicative of adverse RV remodeling) and 13 patients (four men, nine women; mean age, 36 years ± 9) with an RV end-systolic volume index lower than or equal to 72 mL/m^2 (indicative of RV adaptation). Ten adult patients (four men, six women; mean age, 68 years ± 14) with normal cardiac function (based on cardiac MRI results) and no prior history of cardiac disease served as the control group.

Cine Cardiac MRI

Cardiac MRI was performed by using a 1.5-T clinical MRI unit (Gyroscan Intera and Intera; Philips Medical Systems, Best, the Netherlands) equipped with a four-element phased-array coil. Steady-state free-precession MR images were obtained during the imaging sequence, with patients holding their breath for 10–20 seconds. Retrospectively, electrocardiogram gating was performed by using short-axis views encompassing the entire LVs and RVs (approximately 10 images each), with 20 phases per cardiac cycle. The following imaging parameters were used: repetition time msec/echo time msec, 2.8/1.4; flip angle, 45°; section thickness, 8 mm; intersection gap, 0 mm; field of view, 380 × 380 mm^2; acquisition matrix, 176 × 193 pixels; reconstruction matrix, 352 × 352 pixels; and parallel imaging acceleration factor, two. The biventricular end-diastolic volume and biventricular end-systolic volume, which are the sum of the largest and smallest ventricular volumes (in milliliters), respectively, were quantified by using software (Vitrea; Canon Medical Systems, Tochigi, Japan) to perform manual planimetry of the endocardial borders from the short-axis image stack. End-diastolic and end-systolic volumes were indexed to the body surface area, and the ejection fraction percentage was calculated from these two volumes. The stroke volume index was calculated as the difference between the end-diastolic volume index and end-systolic volume index. The cardiac index was calculated as the product of the stroke volume index times the heart rate.

Cardiac MRI Analysis

All images were read in a randomized order, and all readers were blinded to the subject groups. The FDs and strains were semiautomatically calculated by using a common single feature-tracking analysis method, as in a previous study (Fig 1) (15). The image-processing algorithm for cardiac MRI was implemented in MATLAB R2017b, version 9.3 (MathWorks, Natick, Mass) as follows. First, the RV endocardial borders were manually defined as some points at the end of diastole on RV basal, middle, and apical sections on short-axis images (Fig 1, *A*). Endocardium points were then automatically tracked with the assistance of manual correction for a cardiac cycle by using a local template-matching technique based on normalized correlation coefficient values (Fig 1, *B*). In this study, the initial size for the template image and search area was configured to 30 × 30 pixels. However, when the endocardium was not well tracked, the template size and search area were changed to make tracking successful. Finally, the RV blood pool and myocardium were automatically segmented through a cardiac cycle, over a region determined by using spline interpolation of endocardium points. The CS and radial strain
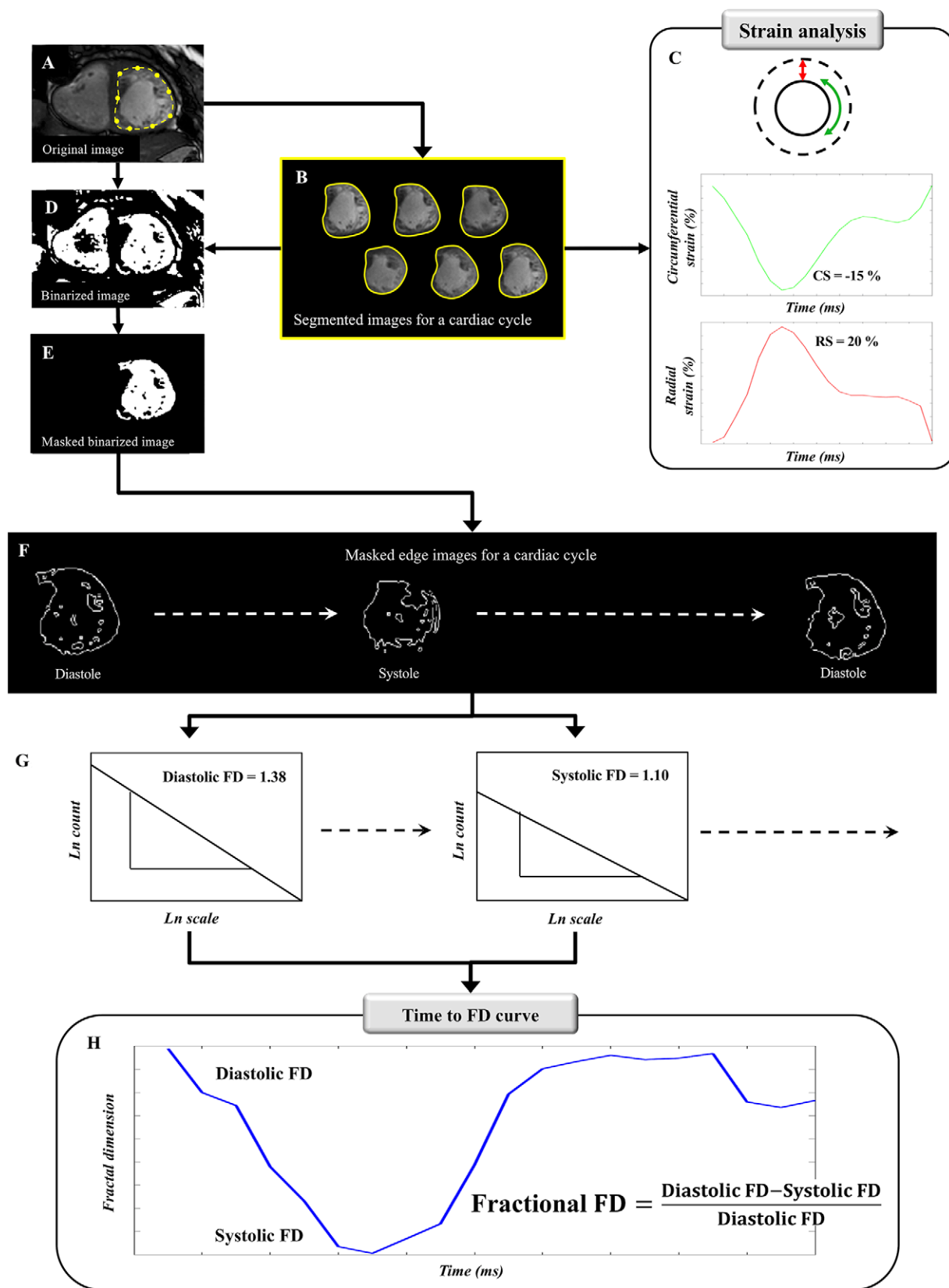
Figure 1:   The workflow for measuring by the strain analysis and the fractal analysis, based on cardiac MRI feature tracking, is shown. Points on the endocardial border, *A*, manually determined at the end of diastole (yellow points), are automatically tracked over one cardiac cycle. *B*, The blood pool and myocardium are then segmented (yellow lines). *C*, Strains are calculated from the edge of the segmented region of the endocardium. Fractal analysis is performed, from the edge image, using automatic processing, and the segmented region (*D-F*), using box-counting method (*G*). *H*, The diastolic fractal dimension (FD) and systolic FD were defined as the maximum and minimum value of the time-FD curve, respectively. The fractional FD is then calculated as the fraction of the changes of FD over a cardiac cycle. CS = circumferential strain, RS = radial strain, Ln = natural logarithm.

(RS) were calculated from the edge of the segmented region of endocardium, with end-systolic CS and RS defined as the peak value of each strain (Fig 1, C). The FDs were calculated from the binarized image (Fig 1, D), with masking of the segmented endocardial regions (Fig 1, E). To ensure standardized processing, binarization was performed automatically by using an adapted threshold method (16). The endocardial border of the binarized image was then extracted by computing edges in the areas of highest gradient magnitude (Fig 1, F) by using the Sobel operator (3 × 3 image gradient operator).

The FDs of the region were calculated over a cardiac cycle by using the standard box-counting method (Fig 1, G), and the time-FD curve was plotted (Fig 1, H). With the standard box-counting method (5), a grid of known spacing (scale) was placed over the endocardial border image (border pixels = 1, background pixels = 0), and the number of boxes that contained nonzero pixels was counted. This process was then repeated for multiple grids with an increase in spacing. As the scale increases, the number of boxes containing the object decreases exponentially, and the exponent is equivalent to the FD. To quantify the exponent, natural logarithmic plots of the number of boxes against scale and the gradient ($-$FD) were estimated by using linear regression. In our method, the maximum spacing (scale) was set to 45% of the diameter of the endocardial border, and the minimum box size was two pixels. *Diastolic FD* (DFD) and *systolic FD* (SFD) were defined as the maximum and minimum values, respectively, of the time-FD curve. The fractional FD (FFD) was then calculated as the fraction of the changes in FD over a cardiac cycle, as follows: FFD = (DFD $-$ SFD)/DFD.

Statistical Analysis

The normality of the data distribution was confirmed by using the Shapiro-Wilk test, and descriptive statistical values—specifically, means and standard deviations—were calculated. One-way analysis of variance, with Tukey post hoc analysis, was used for between-group comparisons. The diagnostic capability of the FD and strain in the detection of adverse RV remodeling was evaluated by using receiver operating characteristic (ROC) analysis. Differences in ROC parameters for different FD cutoffs were compared by using a DeLong test, with one-way analysis of variance used to evaluate between-group differences. Pearson correlation coefficients (r) were calculated between FDs and strain values. All statistical analyses were conducted by using SAS software for Windows, version 13 (SAS Institute, Cary, NC), with statistical significance set at $P < .05$.

Intra- and Interobserver Reproducibility

The intraobserver reproducibility of FD and strain measurements was evaluated by having one observer, who was blinded to the clinical and experimental data, initially perform measurements in 10 randomly selected patients (seven from the cc-TGA group and three from the control group) and then perform repeat measurements at least 1 month after the initial measurements. The order of analysis was randomized independently in the first and second measurements. The interobserver reproducibility of FD and strain measurements were evaluated by having a second observer, who was blinded to the clinical and experimental data, perform measurements in the same 10 patients. Reproducibility was evaluated by using Bland-Altman and intraclass correlation coefficient (ICC) analyses, with one-way (ICC (1, 1)) or two-way (ICC (2, 1)) random single measures. ICCs were defined as excellent (ICC $\geq$ 0.75), good (ICC, 0.60–0.74), moderate (ICC, 0.40–0.59), and poor (ICC $\leq$ 0.39). Intra- and interobserver reproducibility was analyzed in the base, middle region, and apex of the RV.

Results

Comparisons of RV Functional Parameters

The baseline characteristics of the study population are reported in Table 1. Cardiac MRI examinations were successfully performed, with sinus rhythm, in all 19 patients. Patients in the cc-TGA group were significantly younger than individuals in the control group. The RV functional parameters were significantly worse overall in the cc-TGA group than in the control group, with no identified difference between the control and adapted-RV group, with the exception of a relative decrease in the ejection fraction of the RV in the adapted RV group. There were no differences in functional parameter values for the LV among the three groups, with the exception of a relative decrease in the ejection fraction of the LV in the RV-adapted group, as compared with the control group.

Correlations between FDs and RV Remodeling

The areas under the ROC curves for FDs (fractional FD, diastolic FD, and systolic FD) calculated to differentiate patients with adverse RV remodeling are shown in Figure 2. The following ROC values were derived for fractional FD, diastolic FD, and systolic FD at the three RV levels: At the RV base, cutoff values were 0.09, 1.39, and 1.22, respectively; areas under the ROC curve, 0.92 (95% confidence interval [CI]: 0.77, 1.00), 0.63 (95% CI: 0.34, 0.91), and 0.82 (95% CI: 0.59, 1.00), respectively; sensitivity values, 84% (16 of 19), 53% (10 of 19), and 32% (six of 19), respectively; and specificity values, 100% (19 of 19) for all FDs. In the middle RV region, cutoff values were 0.09, 1.39, and 1.24, respectively; areas under the ROC curve, 0.95 (95% CI: 0.82, 1.00), 0.68 (95% CI: 0.40, 0.95), and 0.83 (95% CI: 0.61, 1.00), respectively; sensitivity values, 100% (19 of 19), 32% (six of 19), and 67% (13 of 19), respectively, and specificity values, 95% (18 of 19), 100% (19 of 19), and 100% (19 of 19), respectively. At the RV apex, cutoff values were 0.08, 1.12, and 1.32, respectively; areas under the ROC curve, 0.87 (95% CI: 0.67, 1.00), 0.58 (95% CI: 0.30, 0.87), and 0.69 (95% CI: 0.41, 0.96), respectively; sensitivity values, 84% (16 of 19), 0% (0 of 19), and 16% (three of 19), respectively; and specificity values, 84% (16 of 19), 100% (19 of 19), and 100% (19 of 19), respectively. The areas under the ROC curve for fractional FDs at the RV base, middle region, and apex were significantly greater than those for diastolic FDs and systolic FDs ($P < .01$). Between-group comparisons of the FDs are reported in Table 2.

The following ROC values were calculated for CS and RS at the three RV levels: At the RV base, cutoff values were of -9.3%

Table 1: Baseline Clinical Characteristics of the Study Population

Parameter	cc-TGA Group*			One-Way ANOVA†	Tukey Post Hoc Analysis†		
	RV Remodeling	RV Adapted	Control Group*		Remodeling versus Adapted RV Group	Remodeling versus Control Group	Adapted versus Control Group
No. of patients	6	13	10	32	NA	NA	NA
Age (y)	34 ± 14	36 ± 9	68 ± 14	<.0001‡	.94	<.0001‡	<.0001‡
Male-to-female ratio	4:2	4:9	4:6	NA	NA	NA	NA
BSA (m²)	1.62 ± 0.20	1.57 ± 0.19	1.70 ± 0.20	.39	.87	.79	.35
Systolic blood pressure (mm Hg)	99 ± 13	100 ± 18	120 ± 13	.01‡	.98	.04‡	.02‡
Diastolic blood pressure (mm Hg)	45 ± 16	62 ± 17	62 ± 14	.09	.10	.13	.99
NYHA classification§							
I	…	…	10	NA	NA	NA	NA
II	…	11	…	NA	NA	NA	NA
III	1	2	…	NA	NA	NA	NA
IV	5	…	…	NA	NA	NA	NA
HR (beats/min)	63 ± 13	66 ± 8	62 ± 13	.01‡	.74	.16	.009‡
RV function							
EDVI (mL/m²)	184 ± 82	94 ± 37	84 ± 18	.0005‡	.001‡	.0006‡	.86
ESVI (mL/m²)	117 ± 71	44 ± 16	33 ± 10	.0001‡	.0005‡	.0001‡	.72
EF (%)	38 ± 8	51 ± 7	61 ± 5	<.0001‡	.002‡	<.0001‡	.009‡
SVI (mL/m²)	67 ± 18	49 ± 24	50 ± 9	.16	.17	.23	.99
CAI (L/min/m²)	4.1 ± 1.0	3.3 ± 1.6	3.0 ± 0.5	.23	.35	.22	.90
LV function							
EDVI (mL/m²)	89 ± 16	74 ± 23	81 ± 15	.29	.28	.73	.63
ESVI (mL/m²)	36 ± 11	30 ± 10	28 ± 7	.23	.39	.21	.84
EF (%)	60 ± 6	59 ± 9	66 ± 3	.048‡	.92	.22	.04‡
SVI (mL/m²)	53 ± 6	44 ± 16	54 ± 9	.15	.34	.99	.17
CAI (L/min/m²)	3.3 ± 0.6	2.9 ± 1.1	3.3 ± 0.6	.55	.64	.99	.63

Note.—ANOVA = analysis of variance, BSA = body surface area, CAI = cardiac index, cc-TGA = congenitally corrected transposition of the great arteries, EDVI= end-diastolic volume index, EF = ejection, ESVI = end-systolic volume index, LV = left ventricle, NYHA = New York Heart Association, NA = not applicable, HR = heart rate, RV = right ventricle, SVI = stroke volume index.
*Unless otherwise noted, data are mean values plus or minus standard deviations.
†With the exception of the number of patients, data are *P* values, with *P* < .05 (‡) indicating a statistically significant difference.
§Data are numbers of patients.

and 8.9%, respectively; areas under the ROC curve, 0.92 (95% CI: 0.77, 1.00) and 0.87 (95% CI: 0.67, 1.00), respectively; sensitivity values, 84% (16 of 19) and 68% (13 of 19), respectively; and specificity values, 95% (18 of 19) and 100% (19 of 19), respectively. At the mid-RV region, cutoff values were of −5.5% and 6.6%, respectively; areas under the ROC curve, 0.85 (95% CI: 0.63, 1.00) and 0.86 (95% CI: 0.65, 1.00), respectively; sensitivity values, 52% (10 of 19) for both strains; and specificity values, 100% (19 of 19) for both strains. At the RV apex, cutoff values were of −10.2% and 8.1%, respectively; areas under the ROC curve, 0.90 (95% CI: 0.72, 1.00) and 0.88 (95% CI: 0.70, 1.00), respectively; sensitivity values, 84% (16 of 19) (83%) for both strains; and specificity values, 100% (19 of 19) for both strains.

Correlations between FDs and RV Strains

Pearson correlation coefficients for the correlations between FDs and strains in patients with cc-TGA are reported in Table 3. RV base and mid-RV fractional FD and systolic FD correlated with measured CS and RS. There was no correlation between the diastolic FDs and measured strains. For measurements obtained at the RV apex, there were no correlations between FDs and strains.

Intra- and Interobserver Reproducibility

The intra- and interobserver reproducibility of FD and strain measurements are reported in Table 4. Intra- and interobserver reproducibility was high: All intraclass correlation coefficients
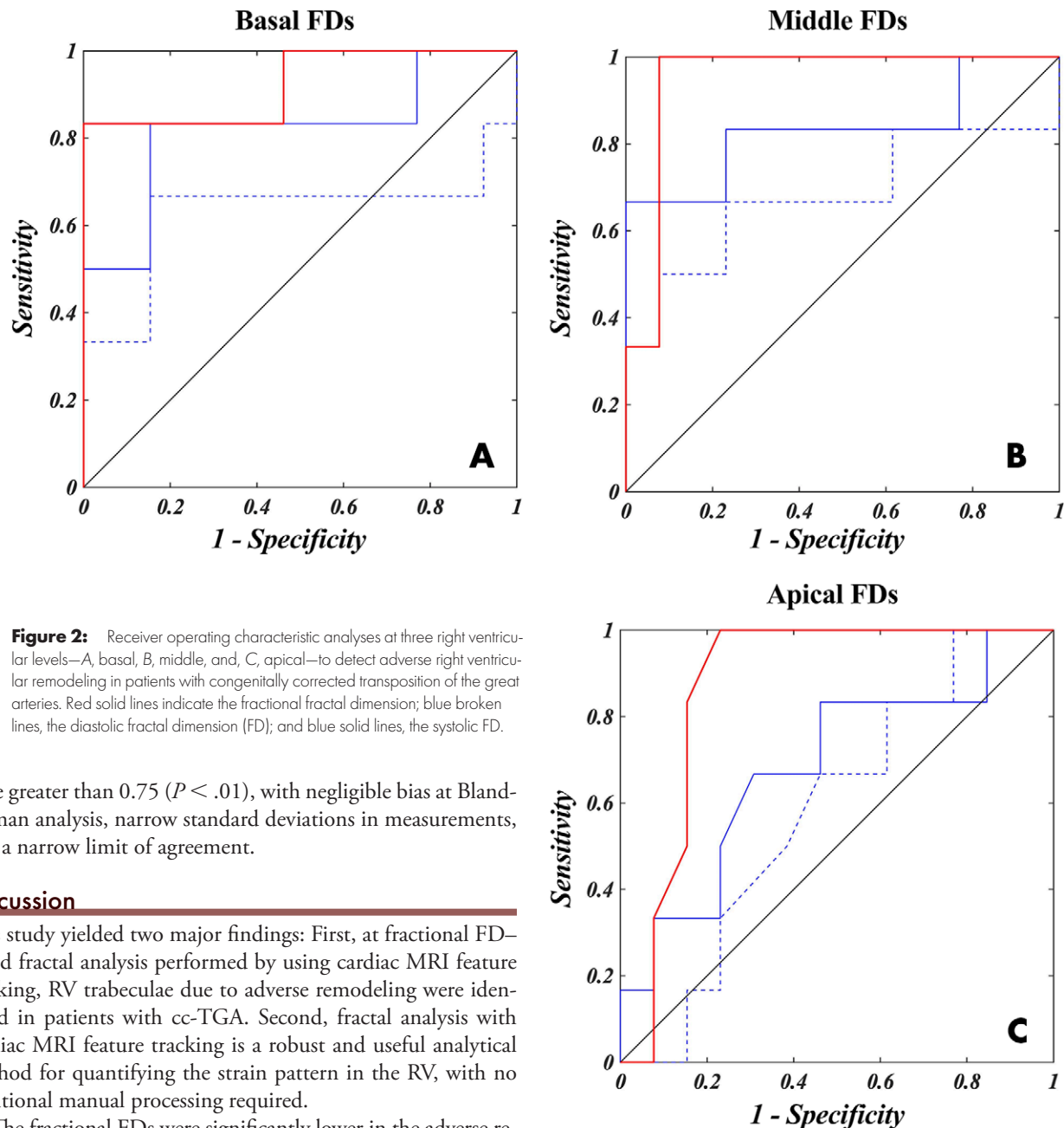
Basal FDs

Middle FDs

Figure 2: Receiver operating characteristic analyses at three right ventricular levels—*A*, basal, *B*, middle, and, *C*, apical—to detect adverse right ventricular remodeling in patients with congenitally corrected transposition of the great arteries. Red solid lines indicate the fractional fractal dimension; blue broken lines, the diastolic fractal dimension (FD); and blue solid lines, the systolic FD.

Apical FDs

were greater than 0.75 ($P < .01$), with negligible bias at Bland-Altman analysis, narrow standard deviations in measurements, and a narrow limit of agreement.

Discussion

This study yielded two major findings: First, at fractional FD–based fractal analysis performed by using cardiac MRI feature tracking, RV trabeculae due to adverse remodeling were identified in patients with cc-TGA. Second, fractal analysis with cardiac MRI feature tracking is a robust and useful analytical method for quantifying the strain pattern in the RV, with no additional manual processing required.

The fractional FDs were significantly lower in the adverse remodeling group than in the adapted RV group. There were no differences in fractional FDs between the cc-TGA group and the control group. The diastolic FD and systolic FD tended to be higher in the patients with cc-TGA, as compared with the control group, with no difference in these FDs between the adverse remodeling and adapted RV groups. Our ROC analyses revealed the high performance of fractional FDs in the diagnosis of adverse RV remodeling compared with the diagnostic performance of the diastolic and systolic FDs. However, for measurements obtained at the RV apex, only the fractional FD enabled differentiation between adapted RV and RV adverse remodeling. Given the detectability of CS for RV adverse remodeling and the substantial decrease in CS associated with adverse RV remodeling, it is likely that residual ventricular trabeculae contribute to greater FDs at systole. As a result, the fractional FD becomes significantly lower in individuals with adverse RV remodeling.

As such, the fractional FD can enable accurate quantification of ventricular trabeculation related to adverse remodeling in the RV apex, where ventricular trabeculae develop prominently (5), and in the basal and middle regions of the RV. In addition, the diagnostic performance of CS was equivalent to that of fractional FD.

In adults with congenital heart disease, it is important to predict the progression of the pathogenesis due to specific hemodynamics and to determine the optimal timing of reoperation during the late phase of the postoperative period (17). The proposed trabecula quantification method is applicable to congenital heart diseases involving right-heart overload such as tetralogy of Fallot, single ventricle, and Ebstein anomaly. Fractal analysis to assess the development of RV trabeculae caused by

Table 2: Comparisons of FD and Strain Values in the RV

| | cc-TGA Group* | | | | Tukey Post Hoc Analysis Results† | | |
Parameter	RV Remodeling	Adapted RV	Control Group*	One-Way ANOVA Results†	RV Remodeling vs Adapted RV Group	RV Remodeling vs Control Group	Adapted RV vs Control Group
RV base							
Fractional FD	0.09 ± 0.03	0.16 ± 0.05	0.12 ± 0.04	.007‡	.008‡	.43	.07
Diastolic FD	1.31 ± 0.10	1.30 ± 0.05	1.20 ± 0.05	.002‡	.94	.007‡	.003‡
Systolic FD	1.19 ± 0.09	1.09 ± 0.06	1.06 ± 0.07	.004‡	.02‡	.004‡	.58
CS (%)	−8.7 ± 1.8	−15.7 ± 4.8	−12.1 ± 3.8	.005‡	.005‡	.26	.10
RS (%)	8.9 ± 3.5	15.4 ± 5.5	14.9 ± 6.0	.06	.06	.11	.97
Middle RV region							
Fractional FD	0.08 ± 0.01	0.14 ± 0.05	0.11 ± 0.04	.01‡	.01‡	.29	.18
Diastolic FD	1.33 ± 0.09	1.30 ± 0.05	1.26 ± 0.06	.10	.79	.12	.20
Systolic FD	1.22 ± 0.09	1.12 ± 0.06	1.12 ± 0.04	.005‡	.007‡	.008‡	.995
CS (%)	−7.4 ± 3.4	−13.6 ± 5.3	−12.0 ± 4.5	.04‡	.04‡	.17	.69
RS (%)	7.5 ± 3.1	13.7 ± 5.2	14.1 ± 4.7	.02‡	.0³‡	.03‡	.98
RV apex							
Fractional FD	0.07 ± 0.01	0.12 ± 0.04	0.13 ± 0.04	.02‡	.04*	.02‡	.81
Diastolic FD	1.33 ± 0.06	1.34 ± 0.09	1.26 ± 0.04	.04‡	.95	.18	.04‡
Systolic FD	1.23 ± 0.07	1.18 ± 0.08	1.10 ± 0.07	.005‡	.37	.005‡	.04‡
CS (%)	−8.1 ± 4.0	−14.8 ± 4.2	−16.1 ± 3.6	.002‡	.007*	.002‡	.74
RS (%)	7.8 ± 3.9	14.3 ± 5.7	15.9 ± 4.2	.01‡	.04*	.01‡	.72

Note.—ANOVA = analysis of variance, cc-TGA = congenitally corrected transposition of the great arteries, CS = circumferential strain, FD = fractional dimension, RS = radial strain, RV = right ventricle.
*Data are mean values ± standard deviations.
†Data are P values, with $P < .05$ (‡) indicating a statistically significant difference.

Table 3: Correlations between FD and Strain Values in Patients with cc-TGA

Parameter	Fractional FD	Diastolic FD	Systolic FD
At RV base			
CS	−0.62 (−0.81, −0.33)*	0.07 (−0.30, 0.43)	0.50 (0.16, 0.73)*
RS	0.50 (0.17, 0.73)*	−0.12 (−0.47, 0.25)	−0.45 (−0.70, −0.10)†
At middle RV region			
CS	−0.70 (−0.85, −0.45 *	0.37 (0.002, 0.65)†	0.78 (0.58, 0.89)*
RS	0.69 (0.44, 0.84)*	−0.38 (−0.66, −0.02)†	−0.78 (−0.89, −0.57)*
At RV apex			
CS	−0.28 (−0.59, 0.10)	0.14 (−0.24, 0.48)	0.30 (−0.07, 0.60)
RS	0.33 (−0.04, 0.62)	−0.16 (−0.49, 0.22)	−0.35 (−0.64, 0.02)

Note.—Data are Pearson correlation coefficients, with 95% confidence intervals in parentheses. cc-TGA = congenitally corrected transposition of the great arteries, CS = circumferential strain, FD = fractional dimension, RS = radial strain, RV = right ventricle.
*$P < .01$.
†$P < .05$, indicating a statistically significant difference.

pulmonary hypertension also has been reported recently (18). Fractal analysis added to standard cardiac function and strain examination is expected to be useful for determining the timing of reoperation in these disease cases. On the basis of our findings, we propose that a fractal analysis–based measurement of trabeculae formation can serve as a sensitive marker of RV remodeling in patients with cc-TGA. By comparison, our findings of greater diastolic and systolic FDs in the cc-TGA group than in the control group in the basal, middle region, and apex of the RV are consistent with previous reports of an increasing RV

Table 4: Intra- and Interobserver Reproducibility of Fractal Analysis and Strain Analysis Data

Parameter	Intraobserver Reproducibility			Interobserver Reproducibility		
	Bias*	SDD	ICC[†]	Bias*	SDD	ICC[†]
RV base						
Fractal analysis						
Fractional FD	−0.15 (−3.64 to 3.34)	1.78	0.89 (0.65, 0.97)	−0.17 (−3.09 to 2.74)	1.49	0.92 (0.70, 0.98)
Diastolic FD	−0.07 (−3.87 to 3.73)	1.94	0.93 (0.75, 0.98)	−0.64 (−2.96 to 1.69)	1.19	0.97 (0.88, 0.99)
Systolic FD	−0.19 (−5.88 to 6.26)	3.10	0.88 (0.60, 0.97)	−0.31 (−4.89 to 4.28)	2.34	0.93 (0.74, 0.98)
Strain analysis						
CS	0.27 (−3.50 to 4.04)	1.92	0.95 (0.83, 0.99)	0.45 (−4.58 to 5.48)	2.57	0.90 (0.65, 0.97)
RS	−0.09 (−2.86 to 2.67)	1.41	0.96 (0.87, 0.99)	−0.35 (−2.63 to 1.93)	1.16	0.98 (0.91, 0.99)
Mid-RV region						
Fractal analysis						
Fractional FD	−0.11 (−5.55 to 3.34)	2.27	0.84 (0.49, 0.96)	−0.20 (−7.84 to 7.83)	3.90	0.84 (0.48, 0.96)
Diastolic FD	−1.24 (−6.61 to 4.13)	2.74	0.83 (0.47, 0.95)	−1.62 (−6.03 to 2.79)	2.25	0.90 (0.65, 0.97)
Systolic FD	0.31 (−4.20 to 4.82)	2.30	0.83 (0.47, 0.95)	−1.28 (−9.11 to 6.56)	4.00	0.95 (0.84, 0.99)
Strain analysis						
CS	1.73 (−4.52 to 7.99)	3.19	0.85 (0.52, 0.96)	0.79 (−6.12 to 7.71)	3.53	0.83 (0.44, 0.95)
RS	−0.33 (−3.02 to 2.37)	1.38	0.95 (0.82, 0.99)	−0.64 (−3.54 to 2.25)	1.48	0.97 (0.89, 0.99)
RV apex						
Fractal analysis						
Fractional FD	−0.30 (−9.45 to 8.86)	4.67	0.92 (0.72, 0.98)	0.57 (−7.72 to 8.87)	4.23	0.81 (0.42, 0.95)
Diastolic FD	−0.82 (−8.78 to 7.15)	4.06	0.93 (0.74, 0.98)	0.23 (−10.70 to 11.16)	5.58	0.85 (0.50, 0.96)
Systolic FD	−0.27 (−17.18 to 16.65)	8.63	0.96 (0.86, 0.99)	−0.43 (−18.61 to 17.74)	9.27	0.96 (0.84, 0.99)
Strain analysis						
CS	−0.02 (−4.96 to 4.92)	2.52	0.87 (0.58, 0.96)	−1.36 (−7.99 to 5.27)	3.38	0.82 (0.43, 0.95)
RS	0.80 (−2.07 to 3.67)	1.46	0.95 (0.82, 0.99)	1.30 (−1.82 to 4.42)	1.59	0.96 (0.85, 0.99)

Note.—Bias and standard deviation of the difference (SDD) of the fractal analysis are expressed as the value times 100. CS = circumferential strain, FD = fractal dimension, ICC = intraclass correlation coefficient, RS = radial strain, RV = right ventricular.
*Numbers in parentheses are limits of agreement.
[†]Numbers in parentheses are 95% confidence intervals.

trabeculation mass with chronic right-heart overload (19). The functional RV parameter values were significantly worse in the adverse RV remodeling group than in both the RV-adapted and control groups, reflecting an exacerbation of right heart-failure in this group.

The advent of adults living with congenital heart conditions is relatively new, reflecting improved surgical management and clinical care of these adults as infants (20). In this study, the highly frequent use of medication for hypertension in this population probably caused the lower blood pressure observed in the cc-TGA group compared with the blood pressure in the control group. In the patients with cc-TGA, significantly greater stroke volume indexes and cardiac indexes were observed, despite their lower RV ejection fractions. This can be explained by RV volume overload or preclinical tricuspid regurgitation. The patients with cc-TGA were significantly younger than the control subjects. However, we believe that there is no difference in RV trabeculae between young and older healthy people. Among the control subjects in this study, the remarkable RV trabeculae were not seen in all cases. Figure

3 shows the results of fractal analysis for one case each in the adverse RV remodeling group (37-year-old man), adapted RV group (40-year-old woman), and control group (67-year-old man). The FDs were relatively high in the patients with cc-TGA (adverse remodeling and adapted), as compared with the FDs in the control group. However, the fractional FDs in the adverse RV remodeling group were smaller (0.09) than those in the adapted RV (0.13) and control (0.12) groups.

An increase in CS of the subaortic RV as an adaptation to the systemic load has been reported (12). Consistent with these results, the CS observed in our study was greater in the adapted RV group than in the control group. Furthermore, fractional FD and systolic FD correlated significantly with CS and RS, which is considered to be a useful marker of systolic function (21). As such, fractional and systolic FDs can serve as sensitive clinical markers of RV remodeling, reflecting specific changes in the contraction pattern with cc-TGA. Therefore, fractional FD–derived fractal analysis based on cardiac MRI feature tracking can facilitate accurate quantification of RV trabeculation associated with adverse remodeling in cc-TGA.
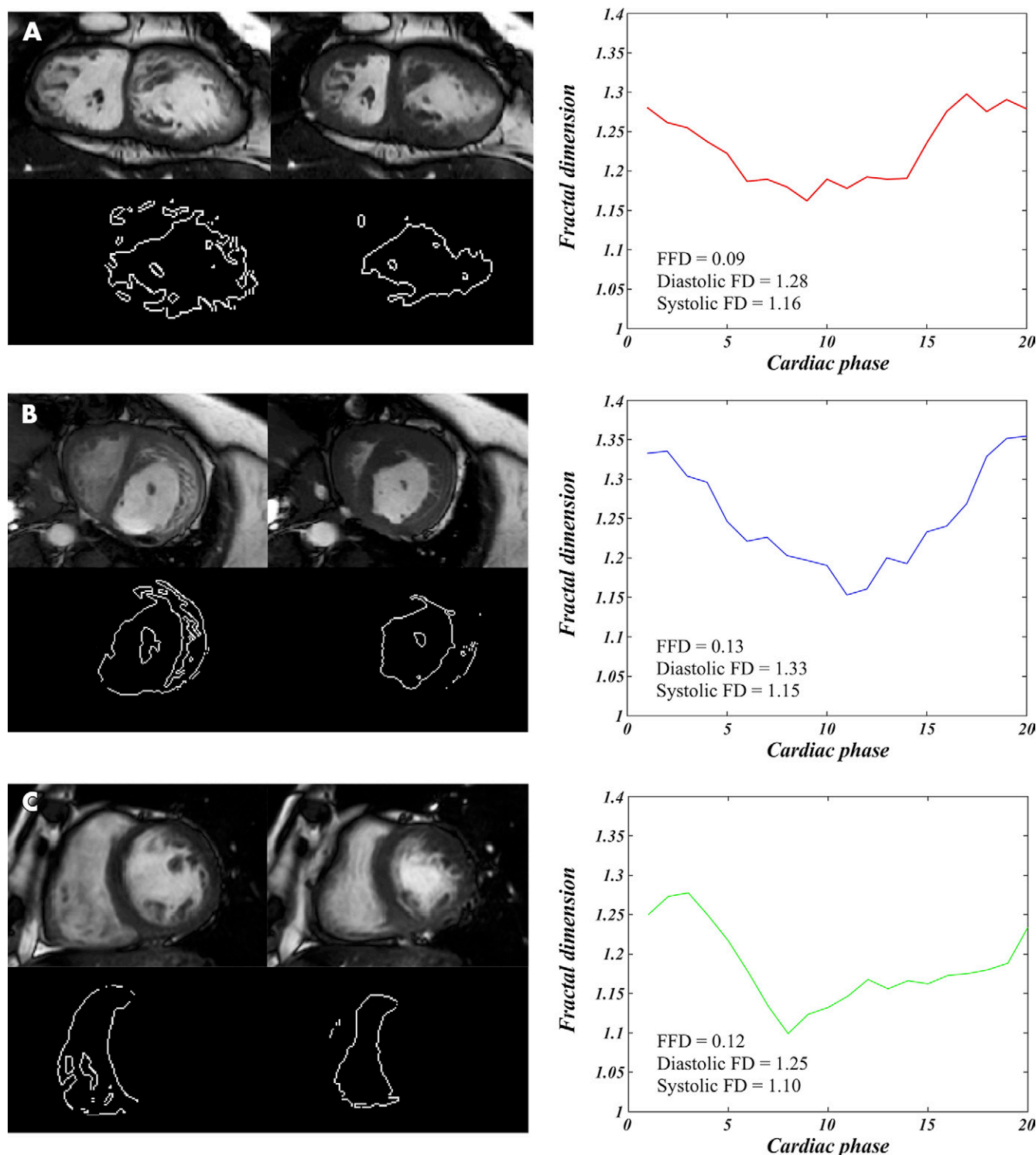
Figure 3: One set of two cine images (upper) and two edge images of the middle portion of the right ventricle (lower) are shown at end-diastole (left) and end-systole (right). Each image set includes a representative case from the, *A*, adverse right ventricular (RV) remodeling group, *B*, the RV adapted group, and, *C*, the control group. The curve of the fractal dimension (FD) for one cardiac cycle is shown for each representative case (right side of *A-C*). The red, blue, and green lines show the FD for the representative case in the adverse RV remodeling, RV adapted, and control groups, respectively. FFD = fractional fractal dimension.

The reproducibility of strain measurements, as assessed with cardiac MR feature tracking has been validated previously (22,23). In addition, the agreement in systolic and diastolic strain measurements between cardiac MR feature tracking and myocardial tagging has been reported (24). We similarly confirmed

high intra- and interobserver reproducibility for fractal analyses, as well as those reproducibilities of strains. Therefore, we consider fractal analysis to be a robust method, with reproducibility equivalent to that of strain analysis. Previous measurements of RV trabeculae obtained by using cardiac MRI were performed

with manual delineation methods (25). With our method, FDs can be derived at routine cardiac cine MRI without additional manual processing for the strain analysis. Diastolic FD, systolic FD, and fractional FD can be fully and automatically calculated by using information from the endocardial region that is extracted by using the feature-tracking technique for strain analysis. This feature, along with the high reproducibility, strongly supports the feasibility and cost-effectiveness of our approach for routine use in clinical practice.

The limitations of our study should be acknowledged. The main limitation was our small sample size, which might have contributed to the lack of significant differences in our comparative analysis of areas under the ROC curve. Recruitment of a larger sample size was limited owing to the rare occurrence of cc-TGA, which accounts for less than 1% of all forms of congenital heart disease (26). Therefore, although we have provided evidence of the promising clinical use of fractal analysis with cardiac MRI feature-tracking for detecting increases in RV trabeculation owing to adverse remodeling, this technique cannot be moved forward before evidence obtained at further analyses with large cohorts is gathered.

Torsion has an important role in cardiac contraction. In this study, the feature-tracking software could not calculate the torsion. Therefore, we were unable to hypothesize a relationship regarding trabeculation compensation for torsion. However, as indicated in a previous study (12), significant correlations between FD and CS values lead us to suspect that there is an association between trabeculation and torsion. In addition, the longitudinal strain was not adapted because it is different from the FD calculation cross-section. We acknowledge that these missing data are a limitation of this study. Another limitation was that the RV remodeling was assessed by using the end-systolic volume index only, according to previous research (14). However, the mechanisms of RV remodeling in congenital heart disease are diverse, and there currently is no clear diagnostic criteria for RV remodeling in the setting of cc-TGA. Our research findings indicate that accurate detection of RV trabeculation in cc-TGA may help elucidate the mechanism of right-heart failure due to adverse remodeling. In addition, the threshold for segmentation of the ventricular blood pool was automatically defined by using the adaptive threshold method (16). We acknowledge that the threshold setting—that is, the initial box size—affects the FD value derived at fractal analysis. In other words, the FD value depends on the spatial resolution of the cardiac MR image (7). If cine imaging with a spatial resolution higher than that of the current imaging examination is used, the FD values and other results may be altered.

In conclusion, fractal analysis based on cardiac MR feature tracking can be used to derive a clinical index of RV remodeling, with changes in the RV strain pattern, and it may prove to be a robust and useful tool for quantifying RV trabeculation due to adverse remodeling in patients with cc-TGA. Once further confirmatory evidence has been gathered, this approach will probably serve as an improved cost-effective and potentially useful tool for the clinical examination of patients with cc-TGA.

Author contributions: Guarantors of integrity of entire study, M.K., U.I., K.I.; study concepts/study design or data acquisition or data analysis/interpretation, all authors; manuscript drafting or manuscript revision for important intellectual content, all authors; approval of final version of submitted manuscript, all authors; agrees to ensure any questions related to the work are appropriately resolved, all authors; literature research, M.K., U.I.; clinical studies, M.K., M.N., U.I., Y.S., K.I., Y.Y., M.Y., S.S.; statistical analysis, M.K., U.I.; and manuscript editing, M.K., M.N., U.I., Y.S., K.I., S.S.

References

1. Dimas AP, Moodie DS, Sterba R, Gill CC. Long-term function of the morphologic right ventricle in adult patients with corrected transposition of the great arteries. Am Heart J 1989;118(3):526–530.
2. Graham TP Jr, Parrish MD, Boucek RJ Jr, et al. Assessment of ventricular size and function in congenitally corrected transposition of the great arteries. Am J Cardiol 1983;51(2):244–251.
3. Ikeda U, Furuse M, Suzuki O, Kimura K, Sekiguchi H, Shimada K. Long-term survival in aged patients with corrected transposition of the great arteries. Chest 1992;101(5):1382–1385.
4. Guihaire J, Haddad F, Mercier O, Murphy DJ, Wu JC, Fadel E. The right heart in congenital heart disease, mechanisms and recent advances. J Clin Exp Cardiolog 2012;8(10):1–11.
5. Captur G, Muthurangu V, Cook C, et al. Quantification of left ventricular trabeculae using fractal analysis. J Cardiovasc Magn Reson 2013;15(1):36.
6. Captur G, Lopes LR, Mohun TJ, et al. Prediction of sarcomere mutations in subclinical hypertrophic cardiomyopathy. Circ Cardiovasc Imaging 2014;7(6):863–871.
7. Captur G, Karperien AL, Li C, et al. Fractal frontiers in cardiovascular magnetic resonance: towards clinical implementation. J Cardiovasc Magn Reson 2015;17(1):80.
8. Schuster A, Hor KN, Kowallick JT, Beerbaum P, Kutty S. Cardiovascular magnetic resonance myocardial feature tracking: concepts and clinical applications. Circ Cardiovasc Imaging 2016;9(4):e004077.
9. Hor KN, Baumann R, Pedrizzetti G, et al. Magnetic resonance derived myocardial strain assessment using feature tracking. J Vis Exp 2011;(48). 2356. doi: 10.3791/2356.
10. Pedrizzetti G, Claus P, Kilner PJ, Nagel E. Principles of cardiovascular magnetic resonance feature tracking and echocardiographic speckle tracking for informed clinical use. J Cardiovasc Magn Reson 2016;18(1):51.
11. Dardeer AM, Hudsmith L, Wesolowski R, Clift P, Steeds RP. The potential role of feature tracking in adult congenital heart disease: advantages and disadvantages in measuring myocardial deformation by cardiovascular magnetic resonance. J Congenit Cardiol 2018;2:3.
12. Pettersen E, Helle-Valle T, Edvardsen T, et al. Contraction pattern of the systemic right ventricle: shift from longitudinal to circumferential shortening and absent global ventricular torsion. J Am Coll Cardiol 2007;49(25):2450–2456.
13. Zheng T, Ma X, Li S, et al. Value of cardiac magnetic resonance fractal analysis combined with myocardial strain in discriminating isolated left ventricular noncompaction and dilated cardiomyopathy. J Magn Reson Imaging 2019;50(1):153–163.
14. Ryo K, Goda A, Onishi T, et al. Characterization of right ventricular remodeling in pulmonary hypertension associated with patient outcomes by 3-dimensional wall motion tracking echocardiography. Circ Cardiovasc Imaging 2015;8(6):e003176.
15. Kawakubo M, Nagao M, Kumazawa S, et al. Evaluation of ventricular dysfunction using semi-automatic longitudinal strain analysis of four-chamber cine MR imaging. Int J Cardiovasc Imaging 2016;32(2):283–289.
16. Bradley D, Roth G. Adaptive thresholding using the integral image. J Graphics Tools 2007;12(2):13–21.

17. Zomer AC, Verheugt CL, Vaartjes I, et al. Surgery in adults with congenital heart disease. Circulation 2011;124(20):2195–2201.

18. Dawes TJW, Cai J, Quinlan M, et al. Fractal analysis of right ventricular trabeculae in pulmonary hypertension. Radiology 2018;288(2):386–395.

19. Vogel-Claussen J, Shehata ML, Lossnitzer D, et al. Increased right ventricular septomarginal trabeculation mass is a novel marker for pulmonary hypertension: comparison with ventricular mass index and right ventricular mass. Invest Radiol 2011;46(9):567–575.

20. Shiina Y, Toyoda T, Kawasoe Y, et al. Prevalence of adult patients with congenital heart disease in Japan. Int J Cardiol 2011;146(1):13–16.

21. Stokke TM, Hasselberg NE, Smedsrud MK, et al. Geometry as a confounder when assessing ventricular systolic function: comparison between ejection fraction and strain. J Am Coll Cardiol 2017;70(8):942–954.

22. Schmidt B, Dick A, Treutlein M, et al. Intra- and inter-observer reproducibility of global and regional magnetic resonance feature tracking derived strain parameters of the left and right ventricle. Eur J Radiol 2017;89:97–105.

23. Alfakih K, Plein S, Thiele H, Jones T, Ridgway JP, Sivananthan MU. Normal human left and right ventricular dimensions for MRI as assessed by turbo gradient echo and steady-state free precession imaging sequences. J Magn Reson Imaging 2003;17(3):323–329.

24. Moody WE, Taylor RJ, Edwards NC, et al. Comparison of magnetic resonance feature tracking for systolic and diastolic strain and strain rate calculation with spatial modulation of magnetization imaging analysis. J Magn Reson Imaging 2015;41(4):1000–1012.

25. Karakus G, Zencirci E, Degirmencioglu A, Güvenc TS, Unal Aksu H, Yildirim A. Easily measurable, noninvasive, and novel finding for pulmonary hypertension: hypertrophy of the basal segment of septomarginal trabeculation of right ventricle. Echocardiography 2017;34(2):290–295.

26. Warnes CA. Transposition of the great arteries. Circulation 2006;114(24):2699–2709.